A&A 394, 663–674 (2002)
DOI: 10.1051/0004-6361:20021147

Astronomy & Astrophysics

On the chaotic rotation of planetary satellites: The Lyapunov spectra and the maximum Lyapunov exponents

I. I. Shevchenko and V. V. Kouprianov

Pulkovo Observatory of the Russian Academy of Sciences, Pulkovskoye ave., 65/1, St. Petersburg, Russia

Received 8 April 2002 / Accepted 24 July 2002

Abstract. The possibility of dynamic chaos in the spin motion of minor natural planetary satellites is studied numerically and analytically. A satellite is modelled as a tri-axial rigid body in a fixed elliptic orbit. The Lyapunov characteristic exponents (LCEs) are used as indicators of the degree of chaos of the motion. For a set of real satellites (i.e. satellites with actual values of inertial and orbital parameters), the full Lyapunov spectra of the chaotic rotation are computed by the HQR-method of von Bremen et al. (1997). A more traditional "shadow trajectory" method for the computation of maximum LCEs is also used. Numerical LCEs obtained in the spatial and planar cases of chaotic rotation are compared to analytical estimates obtained by the separatrix map theory in the model of nonlinear resonance (here: synchronous spin-orbit resonance) as a perturbed nonlinear pendulum (Shevchenko 2000a, 2002). Further evidence is given that the agreement of the numerical data with the separatrix map theory in the planar case is very good. It is shown that the theory developed for the planar case is most probably still applicable in the case of spatial rotation, if the dynamical asymmetry of the satellite is sufficiently small or/and the orbital eccentricity is relatively large (but, for the dynamical model to be valid, not too large). The theoretical implications are discussed, and simple statistical dependences of the components of the LCE spectrum on the parameters of the problem are derived.

Key words. solar system: general – planets and satellites: general – celestial mechanics – chaos

1. Introduction

The calculation of the Lyapunov characteristic exponents (LCEs) is one of the most important tools in the study of chaotic motion, in particular in celestial mechanics. LCEs characterize the rate of divergence of trajectories close to each other in phase space. The quantity reciprocal to the maximum LCE gives the predictability time of the motion. LCEs are closely related to dynamic entropy (Pesin 1976; Benettin et al. 1976; Chirikov 1978, 1979; Meiss 1992).

In this paper, we calculate LCEs of the chaotic rotation of minor planetary satellites. A dynamically asymmetric satellite is considered to be moving in a fixed elliptic orbit. We use the available data on inertial and orbital parameters for a sample of satellites of Mars, Jupiter, Saturn and Neptune. A large fraction of these satellites most probably rotates regularly (in synchronous spin-orbit resonance) at present. However, we always choose starting values of dynamical variables in the chaotic part of phase space to investigate the chaotic regime of rotation, in which every satellite should have resided before being captured into synchronous resonance. Our study covers both cases of planar (the axis of rotation is orthogonal to the orbit plane) and spatial rotation. We compute the full Lyapunov spectra by the HQR-method of von Bremen et al. (1997). For maximum LCE, we also use the traditional "shadow trajectory" method (Lichtenberg & Lieberman 1992).

For a better understanding and control of numerical results, opportunities for analytical estimation of the maximum LCE are explored. This is done in the framework of the model of nonlinear resonance as a perturbed nonlinear pendulum. A method derived by Shevchenko (2000a, 2002) within the separatrix map theory is used to obtain analytical estimates of the maximum LCE in the planar rotation problem. Moreover, we investigate whether these estimates can be used to characterize the spatial chaotic rotation.

2. Definitions and general algorithms

The LCE of a trajectory has the physical meaning of the average divergence rate of trajectories close to the one selected. A nonzero LCE indicates a chaotic character of motion, while an LCE of zero value is the signature of regular (periodic or quasi-periodic) motion.

Let us consider two trajectories close to each other in phase space. One of them we shall refer to as *guiding* and the other as *shadow*. Let $d(t_0)$ be the length of the displacement vector directed from the guiding to the shadow trajectory, at an

Send offprint requests to: I. I. Shevchenko,
e-mail: iis@gao.spb.ru

initial moment t_0. The LCE is defined by the following relation (Lichtenberg & Lieberman 1992):

$$L = \limsup_{\substack{t\to\infty \\ d(t_0)\to 0}} \frac{1}{t-t_0} \ln \frac{d(t)}{d(t_0)}.$$

In the case of a Hamiltonian system, the quantity L may take $2N$ different values (depending on the direction of the initial displacement), where N is the number of degrees of freedom; and LCEs divide into pairs: for each $L_i > 0$ there exists $L_{i+N} = -L_i < 0$, $i = 1, \ldots, N$.

In practical calculations, always an approximation of an LCE over a finite time interval is computed, e.g., an LCE calculated by the so-called shadow trajectory method is given by the formula (Lichtenberg & Lieberman 1992):

$$L_M = \frac{1}{M\Delta t} \sum_{i=1}^{M} \ln r_i, \tag{1}$$

where $r_i = d_i/d_{i-1}$, and d_i stands for the distance between guiding and shadow phase points at the ith step, Δt is the step size, and M is the number of steps at which the distance is measured. While computing the maximum LCE according to Eq. (1), one must perform periodic renormalization of the shadow phase point position with respect to the guiding phase point so that the distance d_i will remain small.

Note that in practical calculations utilizing Eq. (1) one always gets an estimate of just the maximum LCE, because shadow trajectories that can produce any other elements of the LCE spectrum have starting values on a set of measure zero (Lichtenberg & Lieberman 1992). Hence the initial data for a shadow trajectory may be chosen in an arbitrary way, but, of course, such that the separation from the guiding trajectory is sufficiently small.

Consider an algorithm for the computation of the full Lyapunov spectrum in the case of a dynamic system with discrete time. In order to compute the spectrum, one needs to know the tangent map matrix (see von Bremen et al. 1997). Let

$$\boldsymbol{x}_{i+1} = F^{(i)}(\boldsymbol{x}_i) \tag{2}$$

be the original flow map. Then

$$\delta\boldsymbol{x}_{i+1} = \delta F^{(i)}(\delta\boldsymbol{x}_i) \tag{3}$$

is the corresponding tangent map ($\boldsymbol{x}_i$ stands for the phase point position at the ith iteration step, while $\delta\boldsymbol{x}_i$ is the corresponding tangent vector). We shall denote the matrix representation of the tangent map $\delta F^{(i)}$ at the ith step in a standard basis as $J^{(i)}$. Then the approximation of each LCE is given by

$$L_M^k = \frac{1}{M\Delta t} \sum_{j=1}^{M} \ln |r_j^k|, \tag{4}$$

where $r_j^k = R_{kk}^{(j)}$, $k = 1, \ldots, 2N$, and the right-triangular matrix $R^{(j)}$ is obtained iteratively by the QR-factorization of the product $J^{(j)}Q^{(j-1)}$: i.e. $Q^{(j)}R^{(j)} = J^{(j)}Q^{(j-1)}$, where Q is orthogonal and $Q^{(0)}$ is the identity matrix.

The actual LCE is the limiting value of L_M (or L_M^k, if we compute the full Lyapunov spectrum), when $M \to \infty$. In the following the values of L_M (or L_M^k) at large M are taken as authentic values of L (respectively L^k) in all numerical estimates of L in this paper. However, one should emphasize that formally there is a difference. The traditional numerical procedure for finding the limiting values of LCEs (see, e.g., Wisdom 1983) is as follows: when constructing the dependence of $\log L_M$, defined by Eq. (1), upon $\log M$, one finds the value of $\log L_M$ at which the dependence "saturates", i.e. reaches a horizontal plateau. The value of L_M at this plateau is taken as the authentic value of L.

3. Analytical estimation of the maximum Lyapunov exponents

Currently there exist two approaches for estimating maximum LCEs in Hamiltonian systems analytically. The first one (Holman & Murray 1996; Murray & Holman 1997) is essentially based on a method of analytical estimation of the maximum LCE of the standard map, developed by Chirikov (1978, 1979). This method may be called the "standard map approach". The second method (Shevchenko 2000a, 2002), which may be called the "separatrix map approach", takes as its basis the hypothesis by Chirikov (1978, 1979) that the dynamic entropy of the separatrix map is constant in the high-frequency limit of perturbation. A key role in the method belongs to the average dependence of the dynamic entropy of the separatrix map upon λ (the ratio of the perturbation frequency to the frequency of small oscillations on the resonance) in the whole range of λ ($0 < \lambda < +\infty$).

Consider first the standard map approach. Holman & Murray (1996) and Murray & Holman (1997) introduce an effective resonance overlap factor $K_{\rm eff} = (2\pi/\lambda)^2$ for the Hamiltonian of the nonlinear pendulum with symmetric periodic perturbation. This factor is analogous to the stochasticity parameter K of the standard map. Holman & Murray derive estimates of the maximum LCE for the case of a moderate resonance overlap, when $K_{\rm eff}$ is of the order of unity, and for the case of the strong overlap (or, in other words, the case of the low-frequency perturbation limit), when $K_{\rm eff} \gg 1$. In the first case, the maximum LCE is estimated, according to Holman & Murray (1996), as $L \approx \omega_0$ (the frequency of small oscillations on the resonance), and in the second case as $L \approx \Omega$ (the frequency of external perturbation). Murray & Holman (1997) alter somewhat the estimation in the low-frequency limit (the constant Ω is replaced by a logarithmic dependence on $K_{\rm eff}$) and introduce a general approximating formula, which interpolates between the two limits of $K_{\rm eff}$ ($1 < K_{\rm eff} < +\infty$):

$$L = \frac{\Omega}{2\pi} \ln\left(1 + \frac{K_{\rm eff}}{2} + \left(\frac{K_{\rm eff}}{2} + \left(\frac{K_{\rm eff}}{4}\right)^2\right)^{1/2}\right). \tag{5}$$

In the case of the moderate frequency of perturbation $K_{\rm eff} \approx 1$ this formula overestimates the value of the maximum LCE, even in the case of the standard map, by an order of magnitude. The reason is that its derivation is based on a procedure of averaging the tangent map eigenvalues by the phase angle.

In a situation when the measure of the regular component is relatively large, this procedure does not provide adequate results. Due to its limitations, the standard map approach is not used in the following.

Consider the separatrix map approach. In the papers by Shevchenko (2000a, 2002), a method for estimation of the maximum LCE of the motion in a chaotic region in the vicinity of separatrices of perturbed nonlinear resonance was derived in the framework of the separatrix map theory. The perturbed nonlinear resonance is modelled by the following Hamiltonian:

$$H = \frac{\mathcal{G}p^2}{2} - \mathcal{F}\cos\varphi + a\cos(\varphi - \tau) + b\cos(\varphi + \tau), \tag{6}$$

where $\tau = \Omega t + \tau_0$. The variable φ is the resonance phase, p is the conjugate momentum; τ is the phase angle of perturbation, τ_0 is its initial value. The quantity Ω stands for the constant perturbation frequency; $\mathcal{F}$, $\mathcal{G}$, a, b are constants.

The motion close to separatrices is described by the so-called separatrix map. The separatrix map in Chirikov's form (Chirikov 1977, 1978, 1979; Lichtenberg & Lieberman 1992) describes the motion in the vicinity of separatrices of nonlinear resonance subject to symmetric periodic perturbation. Various aspects of a general theory of separatrix maps were considered in Ahn et al. (1995), Treschev (1998), Abdullaev & Zaslavsky (1995, 1996), Vecheslavov (1996, 1999), Shevchenko (1999a, 2000b, 2000c) and many other works. The theory of separatrix maps is of key importance for studies of the chaotic dynamics of celestial bodies. Construction and analysis of separatrix maps constitute a powerful tool of modern nonlinear dynamics. It is primarily oriented at studies of chaotic behaviour.

In the framework of the model of a perturbed nonlinear pendulum, a procedure of reduction of the separatrix map to a unified surface of section of phase space of the original Hamiltonian system (the procedure of synchronization of the map) was derived (Shevchenko 1998a, 2000b). With the help of this procedure, it was shown (Shevchenko 2000b) that separatrix maps provide an adequate description of phase portraits of motion near separatrices both at high and low frequencies of perturbation. General separatrix maps, suitable for the cases of asymmetric perturbations and perturbations characteristic of orbital resonance problems, were derived in applications to problems of celestial mechanics (Shevchenko 1999a, 2000a, 2000c, 2002). In particular, Shevchenko (1999a, 2000a, 2002) applied the separatrix map theory to the construction of phase portraits of the chaotic motion, to analysis of the resonant structure of phase space and to analytical estimation of maximum LCEs in the problem of planar rotational dynamics of an asymmetric satellite moving in an elliptic orbit.

In the case of symmetric perturbation ($a = b$) the separatrix map has two parameters. The first one, λ, is the ratio of Ω, the perturbation frequency, to $\omega_0 = (\mathcal{F}\mathcal{G})^{1/2}$, the frequency of small oscillations on the resonance. The second one (the perturbation parameter) is given by the formula

$$W = \frac{a}{\mathcal{F}}\lambda(A_2(\lambda) + A_2(-\lambda)) = 4\pi\frac{a}{\mathcal{F}}\lambda^2\operatorname{csch}\frac{\pi\lambda}{2}, \tag{7}$$

where

$$A_2(\lambda) = 4\pi\lambda\frac{\exp\frac{\pi\lambda}{2}}{\sinh(\pi\lambda)} \tag{8}$$

is the Melnikov–Arnold integral, as defined by Chirikov (1977, 1979) and Shevchenko (1998a, 2000b).

When the perturbation is asymmetric ($a \neq b$), we have two perturbation parameters instead of W only. These two quantities, W^+ and W^-, are the values of W for the direct and reverse motions of a model pendulum, respectively:

$$\begin{aligned} W^+(\lambda,\eta) &= \varepsilon\lambda\left(A_2(\lambda) + \eta A_2(-\lambda)\right), \\ W^-(\lambda,\eta) &= \varepsilon\lambda\left(\eta A_2(\lambda) + A_2(-\lambda)\right), \end{aligned} \tag{9}$$

where $\varepsilon = \frac{a}{\mathcal{F}}$, $\eta = \frac{b}{a}$.

Following Shevchenko (2000a, 2002), we take the dependence of the maximum LCE of the symmetric separatrix map upon λ in the form

$$h_{sx}(\lambda) \approx C_h\frac{2\lambda}{1+2\lambda}, \tag{10}$$

where $C_h \approx 0.8$ is a constant.

If $a \neq b$, the average period of chaotic rotation (or, equivalently in the approximation of the close-to-separatrix motion, the average half-period of chaotic libration) of the model pendulum is different for the direct and reverse motions:

$$T^{\pm} = \lambda\ln\frac{32e}{\lambda|W^{\pm}|}. \tag{11}$$

The maximum LCEs in the chaotic layer components corresponding to the direct and reverse rotations of the model pendulum, counted per unit of time of the initial Hamiltonian system, are

$$h^{\pm} = \frac{h_{sx}}{T^{\pm}} \tag{12}$$

(Shevchenko 2000a, 2002). Calculation of the mean $\langle h\rangle$ (mean over the whole layer) constitutes a complicated problem. In particular, one should know the relative average times of residence of the system in three different components of the layer corresponding to direct rotation, reverse rotation, and libration of the pendulum. These times depend on the parameters of the system, and on the asymmetry of perturbation among them. Hereafter we take simply

$$\langle h\rangle = \frac{1}{2}\left(h^+ + h^-\right) \tag{13}$$

as the maximum LCE averaged over the layer. This averaging is a rough approximation; however, the derivation of a more precise formula needs a much more complicated and refined theory based on a large amount of numerical experiments with separatrix maps.

The quantities $h^{\pm}$, $\langle h\rangle$ are the maximum LCE per the fraction $\frac{1}{2\pi}$ of the perturbation period of the original Hamiltonian system. In our application, this period is nothing but the orbital period $T_{\rm orb}$ of the satellite. Then the maximum LCE per unit of time (say, a day if $T_{\rm orb}$ is expressed in days) is

$$h_d = \frac{2\pi\langle h\rangle}{T_{\rm orb}}. \tag{14}$$

The time quantity $T_{\rm L} \equiv h_d^{-1}$ is the so-called Lyapunov time. It characterizes the time scale of predictability of the chaotic motion.

So, if the parameters of the separatrix map are known, utilizing Eqs (10)–(14), one can obtain a theoretical estimate of the maximum LCE.

4. Numerical methods for computing the full Lyapunov spectra and maximum LCEs

We use two numerical methods to compute Lyapunov exponents. The traditional "shadow trajectory" method (or, the "two-particle" method) follows straightforwardly from the definition of L_M (Eq. (1)) and is efficient and easy to implement. However, it gives only the maximum LCE, not the full spectrum.

The shadow trajectory method may give false estimates of the LCEs, when the initial shadow trajectory shift is chosen improperly (see, e.g., Tancredi et al. 2001). Namely, LCE estimates obtained by this method may depend on the value of the shadow trajectory initial shift Δx_0. If this shift is too large, then the phase space separation vectors may no longer represent the tangent vectors. The shift cannot be chosen arbitrarily small either, since large numerical errors will emerge when it approaches the machine precision limit. In both cases errors accumulate at renormalization steps. As a result, false estimates of Lyapunov exponents may arise. Tancredi et al. (2001) recommend to verify that there is no dependence of the LCE estimates on Δx_0. We performed such a test and deduced that a shift $\Delta x_0 = 10^{-7}$ is adequate for our problem. As pointed out by Tancredi et al. (2001), it is also important to choose a correct value of the renormalization time interval. If this is chosen too small, it can increase the accumulation of roundoff errors due to more frequent renormalizations. If it is too large, a numerical overflow may occur. We tried various values for the renormalization step size (see below). Choosing it equal to the iteration step size appears to be adequate in all cases.

The second method is that proposed by von Bremen et al. (1997). It is based on the QR-decomposition of the tangent map matrix defined by Eq. (3). It utilizes the Householder transformation. It is therefore known as the HQR method. Von Bremen et al. (1997) proved it to be more numerically stable than the Gram–Schmidt (GS) orthogonalization procedure involved in the method by Benettin et al. (1976). The HQR method by von Bremen et al. (1997) is also more efficient compared to other factorization procedures. It is less sensitive to the iteration step size, because it does not require renormalization. In what follows, Lyapunov spectra are computed by the HQR method by von Bremen et al. (1997).

If the tangent map matrix $J^{(i)}$ is not given analytically, there are two ways to calculate it. First, one may replace the tangent vectors $\delta\boldsymbol{x}_i$ in Eq. (3) with small displacement vectors: $\Delta\boldsymbol{x}_i = \boldsymbol{x}'_i - \boldsymbol{x}_i$, where $\boldsymbol{x}_i$ and $\boldsymbol{x}'_i$ are the guiding and the shadow phase point, respectively, at the integration step i. Then both points are iterated independently using Eq. (2). This gives $\Delta\boldsymbol{x}_{i+1} = \boldsymbol{x}'_{i+1} - \boldsymbol{x}_{i+1}$. Having repeated this procedure for $2N$ linearly independent vectors $\Delta\boldsymbol{x}_i$, one can solve the equation

$$\Delta\boldsymbol{x}_{i+1} = J^{(i)}\Delta\boldsymbol{x}_i \tag{15}$$

with respect to the tangent map matrix $J^{(i)}$. This method requires only knowledge of the initial flow map (2). Dependence of results on the initial shadow trajectory shift is not so critical here, as in the method by Benettin et al. (1976). The reason is that all shadow particles are reset to their initial positions at each step. Therefore, there is no roundoff error accumulation due to renormalizations. The method described is used for the majority of LCE computations in this paper.

We note that the tangent map matrix can be found with a higher precision, but at much greater computation cost, if one computes the tangent map directly, by means of simultaneous integration of the original and linearized systems. This approach does not need the introduction of an auxiliary small shift parameter Δx_0. We shall explore this opportunity in future work[1].

The computational efficiency of the method employed in this paper is decreased by the necessity to perform $2N$ additional iterations of the flow map at each step. However, an extra opportunity exists to compute the tangent map matrix. This opportunity is appropriate when the flow map (2) is given by an original continuous dynamic system

$$\boldsymbol{x}' = F(\boldsymbol{x}, t). \tag{16}$$

Then the tangent map matrix is approximated by

$$J^{(i)} = I + \nabla_{\boldsymbol{x}} F(t_i) \cdot \Delta t, \tag{17}$$

where $\nabla_{\boldsymbol{x}} F(t_i)$ is the Jacobi matrix of the system at $t = t_i = i\Delta t$, and I is the unity matrix. This approximation, however, is valid only when the iteration step Δt is sufficiently small. This method of calculating the tangent map matrix is used in what follows only for testing purposes.

Generally, we probed the values of the iteration step $\Delta t = 0.01\cdot 2\pi$, $\Delta t = 0.1\cdot 2\pi$ and $\Delta t = 1$. The step size made practically no difference in the case of the HQR method, though smaller step sizes seem slightly preferable.

A complementary test of the validity of the calculation of the full Lyapunov spectrum is to compute the sum of all exponents $\sum_{k=1}^{2N} L^{(k)}$. Hereafter $N = 3$, and we shall denote the sum as $\sum^{(6)} L$ for brevity. The sum ought to be equal to zero (see Sect. 2). It was monitored to estimate the intrinsic precision of the method. This precision can be affected by the choice of the initial shadow particle shift or iteration step size, as well as by the quality of the integrator employed.

5. Lyapunov exponents for the chaotic rotation of planetary satellites

A large fraction of natural satellites whose dimensions are less than 500 kilometers has a definitely asymmetric geometric shape (see, e.g., tables in Éphémérides Astronomiques 1995). Most of the information on the geometric form of satellites is derived nowadays from photographic data obtained in interplanetary missions.

Many known planetary satellites rotate in synchronous resonance with their orbital motion. Indeed, planar rotational motion (in the orbital plane) in synchronous resonance, as inferred in the theory of tidal spin-orbit interaction (see, e.g., Beletsky 1981; Wisdom 1987), is the natural final stage of the long-term dynamical evolution of a satellite. At this stage, the rotation axis is coincident with the axis of the maximum moment of inertia.

[1] We are thankful to Dr. D. J. Scheeres for the suggestion to consider this approach.

However, when, in the course of the long-term dynamical evolution, the phase trajectory comes close to the separatrices of synchronous resonance and enters the chaotic layer formed by the split separatrices, the satellite starts to perform chaotic tumbling, since the planar rotation in this domain of phase space is unstable with respect to tilting the axis of rotation (Wisdom et al. 1984; Wisdom 1987; Melnikov & Shevchenko 1998, 2000). Then the satellite rotates chaotically by all Euler angles. The greater the dynamical asymmetry and the orbital eccentricity of the satellite, the greater the domain of the chaotic motion in phase space; though the roles of these two parameters are very different.

As Wisdom (1987) pointed out, for a satellite to be caught in synchronous resonance the passage through the domain of instability should be sufficiently fast; the width of the chaotic layer should be correspondingly narrow. Of course, the motion in the center of synchronous resonance itself should be stable with respect to tilting the axis of rotation. In the course of dynamical evolution, a satellite passes through various resonant spin-orbit states and the chaotic layers near their separatrices. Estimates of maximum LCEs in these layers can provide information on the character of the dynamical evolution.

Up to now only Hyperion, the seventh satellite of Saturn, has been observationally confirmed to be in a state of chaotic rotation (Klavetter 1989; Black et al. 1995; Devyatkin et al. 2002). A major fraction of other satellites is probably in a regular state close to synchronous (Peale 1977). In any case, capture in synchronous resonance cannot be accomplished without passage through the main chaotic layer, therefore the knowledge of maximum LCEs in this layer can be helpful for studies of the dynamical history of satellites. Depending on the scenario, analytical estimates of LCEs can be recalculated for values of the eccentricity corresponding to selected moments of the dynamical evolution.

In the case of satellites with chaotic or unknown rotational dynamics, theoretical estimates of LCEs provide useful information for planning observational studies of these dynamics. A practically unique opportunity for ground-based studies remains the construction and analysis of the lightcurves of satellites (Klavetter 1989; Devyatkin et al. 2002). The reciprocal of the maximum LCE (the Lyapunov time) gives the predictability time of chaotic rotation. It is clear that if the observational goal is the study of rotational dynamics, possibly chaotic, the typical interval between observations should be less than the Lyapunov time. This imposes important restrictions on the frequency of observations.

In this section we consider the chaotic regime of rotation of 11 selected satellites. These are the satellites for which estimates of the necessary inertial and orbital parameters could be found in literature. Currently, among these satellites only Hyperion is known to rotate chaotically (most probably; see Klavetter 1989; Black et al. 1995; Devyatkin et al. 2002). For five satellites (Helene, Atlas, Prometheus, Pandora and Proteus) the type of rotation is unknown. The rotation of Phobos, Deimos, Amalthea, Epimetheus, and Janus is known to be regular, each of them being in synchronous resonance (see, e.g., Peale 1977; Wisdom 1987). We include the satellites with an actual regular mode of rotation in our analysis, but set the starting values for integration in the chaotic domain of phase space (namely, close to separatrices of synchronous resonance). In other words, we study the possible regime of rotation of a satellite which takes place in case the satellite were not caught in synchronous resonance. All satellites are included in order to obtain more representative statistics for comparison with theory and between various cases of dynamics; besides, the satellites with current regular rotation should have been in the chaotic mode at some stage of their dynamical history, before they were caught in synchronous resonance. The passage of the chaotic domain close to separatrices of synchronous resonance in the course of the tidal dynamical evolution is unavoidable. However, the orbital eccentricities during this passage could be different, but, as one cannot judge their values at that time, we take the present values.

Actual values of the LCEs of chaotic rotation could be different from what we expect as well for another reason. All satellites move in unperturbed elliptic orbits. It is well known, however, that in reality the elements of their orbits are subject to perturbations due to oblateness of the central planet and/or due to the existence of other massive satellites. E.g., in case of Hyperion, the eccentricity of the orbit oscillates from ≈0.08 to ≈0.12 with a period of 18.8 years (Black et al. 1995), due to perturbations from Titan. The Lyapunov times calculated in what follows are equal to a few days in the majority of cases. This is much less than the time scale of the strong long periodic perturbations. Therefore taking into account such perturbations seems to be superfluous.

5.1. The case of planar rotation

Consider the motion of an asymmetric rigid body ("satellite") about its mass center moving in an unperturbed elliptic orbit around a "planet" (a motionless gravitating point). We assume that the satellite dimensions are much less than the radius of its orbital motion, its mass being negligible compared to the mass of the planet. The principal moments of inertia of the satellite in relation to its axes of inertia a, b, c are denoted as A, B, C respectively. The axes are chosen in such a way that $A < B < C$. (Note that a is used in what follows also as a designation for the semimajor axis of the orbit. This should not be confusing since the meaning of a is determined by the context.)

In this section, we compare numerical estimates of the maximum LCEs with theoretical ones in the problem of the planar chaotic rotation of a satellite moving in a fixed elliptic orbit. The axis of rotation of a satellite is set to coincide with that of its maximum moment of inertia. It is orthogonal to the orbit plane. The rotational motion is then described by the Beletsky equation (Beletsky 1965) for the planar librations/rotations of a satellite in an elliptic orbit. In the case of small eccentricities, the equations of motion are given by the Hamiltonian (6), which is derived neglecting all powers of the eccentricity higher than unity (see, e.g., Wisdom et al. 1984; Celletti 1990). According to Shevchenko (2000a, 2002), one has for the pendulum paradigm: $\mathcal{F} = \frac{\omega_0^2}{4}$, $\mathcal{G} = 4$, $\Omega = 1$, $a = -\frac{7e\omega_0^2}{8}$, $b = \frac{e\omega_0^2}{8}$, $\varepsilon = -\frac{7e}{2}$; the inertial parameter $\omega_0 \equiv \left(\frac{3(B-A)}{C}\right)^{1/2}$, where $A < B < C$ are the principal central moments of

inertia of the satellite; e is the eccentricity of the orbit. In what follows, time is measured in units of $\frac{1}{2\pi}$ of the orbital period.

The flow map (2) is generated by the equations of motion. The integrator used is that of Hairer et al. (1987). It is an explicit Runge–Kutta method of order 8 due to Dormand and Prince (see Hairer et al. 1987) with step size control and dense output. The integrations were performed within the time interval $t \in [0, 10^5]$. This choice proved to be sufficient for the dependence of L versus t to saturate (reach a plateau). The starting values for the integrations were chosen to lie inside the chaotic domain of phase space.

Figure 1 shows the numerical estimates of maximum LCEs for $e = 0.1$, which is the mean eccentricity of the orbit of Hyperion (see, e.g., Wisdom et al. 1984). The dynamical asymmetry parameter ω_0 is taken in the range $0.2 \le \omega_0 \le 1$. The corresponding theoretical curve according to Eqs. (10)–(13) is given for comparison with the numerical data.

Let us now compare the numerical estimates of the maximum LCEs with theoretical ones for the set of 11 satellites already mentioned above. The satellites are listed in Table 1. The values of the inertial parameters A/C, B/C (or the values of the geometrical dimensions a, b and c; then A/C, B/C are determined in the model of an ellipsoid with homogeneous density) and the orbital eccentricities are taken from the papers by Simonelli et al. (1993) for Phobos; Wisdom (1987) for Deimos, Amalthea, Janus and Epimetheus; Thomas et al. (1995) for Hyperion; Smith et al. (1982) for Helene; Burša (1990) for Atlas; Goździewski & Maciejewski (1995) for Prometheus and Pandora; Éphémérides Astronomiques (1995) for Proteus. The values of A/C, B/C (necessary for computations of spatial rotation and presented below in Table 3) determine the value of the parameter ω_0 (given in Table 1): $\omega_0 = \left(\frac{3(B-A)}{C}\right)^{1/2}$.

A graphic comparison of numerical estimates of the maximum LCEs with theoretical ones for our set of satellites is given in Fig. 2. The theoretical estimates of maximum LCEs are calculated using the separatrix map theory by Shevchenko (2000a, 2002) (see Sect. 3). The numerical estimates are averages of the current LCE over the time interval $t \in [5 \times 10^4, 10^5]$ corresponding to the LCE saturation plateau. Two values of Δt were used in computations (see Table 1). In the two cases the agreement with theory is almost equally good. The data for $\Delta t = 0.01 \cdot 2\pi$ are used in constructing the graph.

Both Figs. 1 and 2 demonstrate that the numerical values and the theory are in good agreement in the case of planar rotation.

In Table 2, we present the results of computations of the full Lyapunov spectra of the planar rotation. The HQR method is used. Note that the virtual shadow trajectories in the HQR method are not confined to the orbit plane. Therefore $L^{(2)}$ and $L^{(3)}$ are not necessarily zero. Instead of the equations of motion defined by the Hamiltonian (6), we use the Euler equations (see Sect. 5.2). As defined above, the iteration step size is $\Delta t = 0.01 \cdot 2\pi$, the initial shadow particle separation is $x_0 = 10^{-7}$. As already adopted, the LCEs are averages over the time interval $t \in [5 \times 10^4, 10^5]$. The mean values of the positive LCEs and the absolutes of their negative counterparts are presented, i.e., by $L^{(i)}$ we imply $\frac{1}{2}(L^{(i)} + |L^{(i+N)}|)$. The sum

Table 1. The case of planar rotation. The inertial parameter, orbital eccentricity and numerical estimates of the maximum LCE by the shadow trajectory method.

Satellite	ω_0	e	Maximum LCE	
			$\Delta t = 1$	$\Delta t = \frac{2\pi}{100}$
Phobos (M1)	.617	.01500	.059	.060
Deimos (M2)	.812	.00050	.034	.041
Amalthea (J5)	1.139	.00300	.060	.061
Hyperion (S7)	.887	.10000	.119	.117
Janus (S10)	.661	.00900	.041	.049
Epimetheus (S11)	.780	.00700	.053	.060
Helene (S12)	.593	.00500	.047	.038
Atlas (S15)	.467	.00200	.033	.026
Prometheus (S16)	1.175	.00400	.064	.069
Pandora (S17)	.934	.00400	.059	.055
Proteus (N8)	.376	.00046	.025	.025

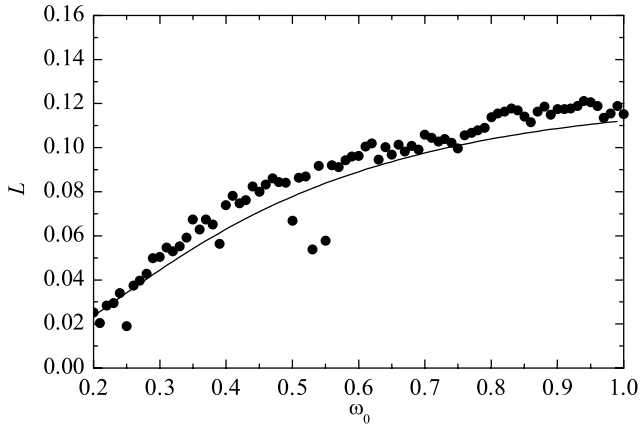

Fig. 1. Comparison of numerical (circles) and theoretical (curve) estimates of the maximum LCE in the case of Hyperion's orbital eccentricity.

$\sum^{(6)} L$, which was calculated to test the consistency of the HQR method, turned out to be equal to zero up to the 6th decimal digit, for all satellites.

To give an idea of the saturation time for computing the Lyapunov exponents, we present the dependences of the current LCEs on time in the case of Hyperion in Fig. 3.

As one can see from a comparison of Tables 1 and 2, the values of maximum LCEs obtained by the shadow trajectory method and those of $L^{(1)}$ computed by the HQR method are in agreement.

5.2. The case of spatial rotation

Let us define a reference frame x, y, z at the pericenter of the satellite orbit, in the following way: the x axis is directed along the line "pericenter–planet", the y axis is parallel to the vector of orbital velocity, the z axis is orthogonal to the orbital plane and completes the reference system to a right-handed system. Orientation of the satellite in this frame is defined by a sequence of imaginary rotations of the satellite by the Euler

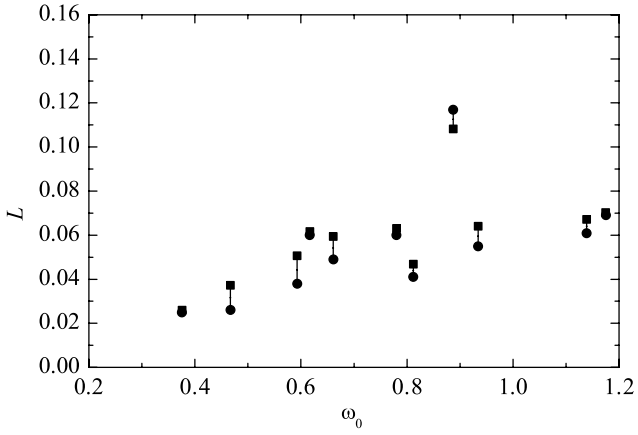

Fig. 2. Comparison of numerical (circles) and theoretical (squares) estimates of the maximum LCE for 11 satellites.

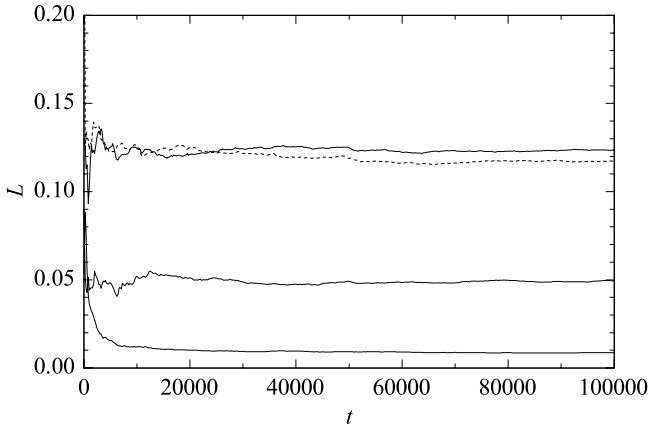

Fig. 3. The current maximum LCE (obtained by the shadow trajectory method; dashed line) and the current Lyapunov spectrum (obtained by the HQR method; solid line) versus time for Hyperion; the planar case.

Table 2. The case of planar rotation. Numerical estimation of the Lyapunov spectra by the HQR method.

Satellite	$L^{(1)}$	$L^{(2)}$	$L^{(3)}$
Phobos	.051	.035	.0019
Deimos	.040	.030	.0081
Amalthea	.064	.039	.0036
Hyperion	.123	.049	.0087
Janus	.049	.031	.0018
Epimetheus	.060	.033	.0025
Helene	.046	.024	.0012
Atlas	.036	.024	.0017
Prometheus	.066	.032	.0165
Pandora	.057	.038	.0091
Proteus	.024	.010	.0003

angles θ, ϕ, ψ from an initial position until the satellite reaches its actual orientation. In the initial position, the axes of inertia a, b, c are directed along axes x, y, z, respectively. The sequence of the imaginary rotations is chosen to have the following order: first, one makes a rotation by θ about z, then by ϕ about a, and, finally, by ψ about b. The same coordinate system was used, e.g., by Wisdom et al. (1984).

The angular velocity vector $\boldsymbol{\omega}$ of the satellite rotating in the planet gravity field is described by the Euler dynamic equations (see, e.g., Beletsky 1965; Wisdom et al. 1984):

$$\begin{aligned} A\frac{\mathrm{d}\omega_a}{\mathrm{d}t} - \omega_b\omega_c(B-C) &= -3\frac{GM}{r^3}\beta\gamma(B-C), \\ B\frac{\mathrm{d}\omega_b}{\mathrm{d}t} - \omega_c\omega_a(C-A) &= -3\frac{GM}{r^3}\gamma\alpha(C-A), \\ C\frac{\mathrm{d}\omega_c}{\mathrm{d}t} - \omega_a\omega_b(A-B) &= -3\frac{GM}{r^3}\alpha\beta(A-B), \end{aligned} \tag{18}$$

where G is the universal constant of gravity; M is the mass of the planet; r is the distance "satellite – planet"; ω_a, ω_b, ω_c are the components of the angular velocity vector $\boldsymbol{\omega}$ in the a, b, c frame; α, β, γ are the direction cosines of the principal axes of inertia relative to the direction to the planet. According to Wisdom et al. (1984), in the adopted coordinate system, the direction cosines are as follows:

$$\begin{aligned} \alpha &= \cos\psi\cos(\theta-f) - \sin\psi\sin\phi\sin(\theta-f), \\ \beta &= -\cos\phi\sin(\theta-f), \\ \gamma &= \sin\psi\cos(\theta-f) + \cos\psi\sin\phi\sin(\theta-f). \end{aligned} \tag{19}$$

Note that the expressions for the moments of gravity forces (the right-hand parts of Eqs. (18)) are valid if the satellite dimensions are small compared to r.

The Euler kinematic equations in the same coordinate system, according to Wisdom et al. (1984), reduce to

$$\begin{aligned} \frac{\mathrm{d}\theta}{\mathrm{d}t} &= \frac{\omega_c\cos\psi - \omega_a\sin\psi}{\cos\phi}, \\ \frac{\mathrm{d}\phi}{\mathrm{d}t} &= \omega_a\cos\psi + \omega_c\sin\psi, \\ \frac{\mathrm{d}\psi}{\mathrm{d}t} &= \omega_b - (\omega_c\cos\psi - \omega_a\sin\psi)\tan\phi. \end{aligned} \tag{20}$$

Simultaneous integrations of the dynamic and kinematic Euler Eqs. (18), (20) give the evolution of the orientation of the satellite, i.e. the angles θ, ϕ, ψ as a function of time.

Hereafter we measure time in units of $\frac{1}{2\pi}$ of the orbital period, as in Sect. 5.1.

The value of r in Eqs. (18) is given by the relation $r = a(1 - e\cos E)$, where E is calculated by solving the Kepler equation. We use the usual notations for the orbital elements: a stands for the semimajor axis, e for the eccentricity. The position of the body in its orbit is given by the true anomaly f, or, alternatively, by the eccentric anomaly E.

The numerical estimates of the Lyapunov exponents are calculated here by integrating the Euler equations under the following initial conditions: $\theta|_{t=0} = 1.5$, $\phi|_{t=0} = 0.001$, $\psi|_{t=0} = 0.001$, $\dot\theta|_{t=0} = 1$, $\dot\phi|_{t=0} = 0$, $\dot\psi|_{t=0} = 0$. A small shift in $\phi|_{t=0}$ and $\psi|_{t=0}$ from zero values is introduced to bring the motion out of the orbit plane. The eccentricity e of the satellite and the ratios A/C, B/C of its moments of inertia are the parameters of the problem.

We use both the shadow trajectory method and the HQR method. The integrator and the iteration step sizes are the same as in the planar case. The number of iterations in the spatial

Table 3. The case of spatial rotation. The inertial parameters, orbital eccentricity and numerical estimates of the maximum LCE by the shadow trajectory method.

Satellite	A/C	B/C	e	Max. LCE
Phobos	.7234	.8504	.01500	.067
Deimos	.6612	.8808	.00050	.164
Amalthea	.5049	.9371	.00300	.120
Hyperion	.6220	.8840	.10000	.085
Janus	.7302	.8757	.00900	.074
Epimetheus	.7055	.9081	.00700	.079
Helene	.8293	.9466	.00500	.064
Atlas	.7493	.8220	.00200	.121
Prometheus	.4124	.8723	.00400	.164
Pandora	.5717	.8622	.00400	.128
Proteus	.9215	.9685	.00046	.031

Table 4. The case of spatial rotation. Numerical estimation of the Lyapunov spectrum by the HQR method, and the sum of all LCEs.

Satellite	$L^{(1)}$	$L^{(2)}$	$L^{(3)}$	$\sum^{(6)} L$
Phobos	.084	.026	.0059	.00035
Deimos	.160	.040	.0058	.00017
Amalthea	.110	.038	.0080	.00051
Hyperion	.080	.031	.0083	.00086
Janus	.086	.029	.0061	.00021
Epimetheus	.081	.027	.0054	.00039
Helene	.049	.017	.0033	.00022
Atlas	.125	.030	.0055	.00007
Prometheus	.128	.051	.0101	.00091
Pandora	.092	.031	.0054	.00046
Proteus	.040	.004	.0005	0

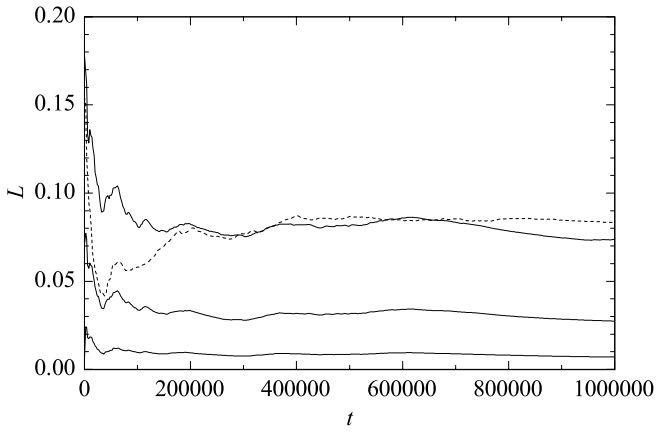

Fig. 4. The current maximum LCE (obtained by the shadow trajectory method; dashed line) and the current Lyapunov spectrum (obtained by the HQR method; solid line) versus time for Hyperion; the spatial case.

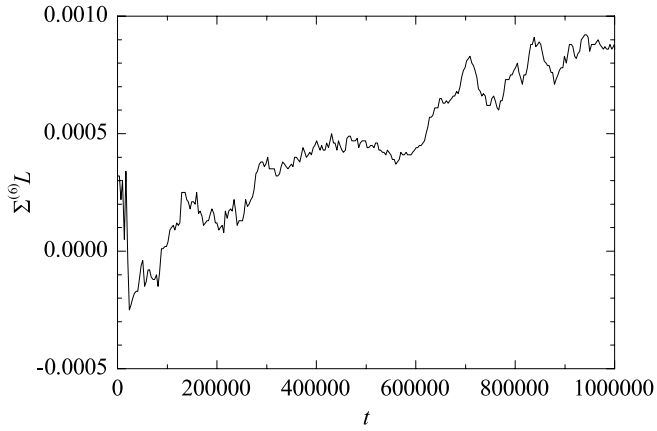

Fig. 5. The sum of all LCEs versus time for Hyperion; the spatial case.

case should, however, be greater than in the planar case, since the topology of chaotic domains in phase space is much more complicated now, and therefore it takes much longer for the $L^{(i)}$ to saturate. One should average over longer time scales in order to obtain true LCE estimates. On the other hand, the sum $\sum^{(6)} L$, which is an indicator of accumulation of errors, grows more rapidly. In our experience, the dependences saturate after $t_M = 5 \times 10^5$ for all satellites. So, we averaged current LCEs on the time interval $t \in [5 \times 10^5, 10^6]$.

In Table 3, we present numerical estimates of the maximum LCEs (by the shadow trajectory method) of spatial rotation for 11 satellites described in Sect. 5.1.

In Table 4, we present the results of the calculations of the full Lyapunov spectra in the case of spatial rotation. The integration parameters are the same as in Sect. 5.1. The last column contains the values of the sum $\sum^{(6)} L$ (an indicator of accumulation of errors) at the final iteration step t_M. We should point out that the contributions of the individual pair sums $L^{(i)}+L^{(i+N)}$ $(i = 1, \ldots, 3)$ to the total sum $\sum^{(6)} L$ appeared to be of the same order, so an error present in each $L^{(i)}$ can be taken approximately as $\left|\sum^{(6)} L\right|/3$.

Just like in Sect. 5.1, we show dependences of the LCEs on time for Hyperion in Fig. 4. In Fig. 5, a graph of the sum $\sum^{(6)} L$ versus time is presented; one can see how the errors accumulate on long time scales.

Our LCE spectrum for Hyperion can be compared to the results of Wisdom et al. (1984), though we use slightly different data (due to Thomas et al. 1995) for the values of the moments of inertia of this satellite. Wisdom et al. (1984) show a computed dependence of current LCEs for the case of spatial rotation of Hyperion, upon time of computation, in Fig. 9 of their article. A close resemblance to our numerical data is seen, though the details of the graphs are of course different, mainly due to different times of computation.

6. Comparison of the cases of planar and spatial rotation

Let us first compare the results of calculations of the maximum LCEs in the shadow trajectory method with those in the HQR method.

In Fig. 6 we present the graph of the Lyapunov exponent $L^{(1)}$ (obtained by the HQR method) versus the maximum LCE L (obtained by the shadow trajectory method) for the selected 11 satellites. The rotation is planar. The values of $L^{(1)}$

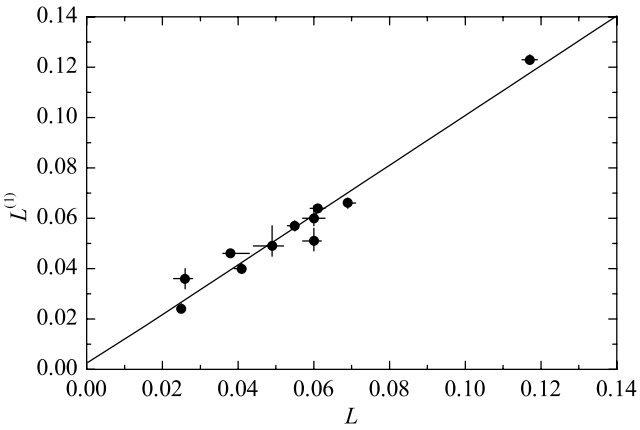

Fig. 6. The maximum LCEs computed by different methods; 11 satellites; the planar case.

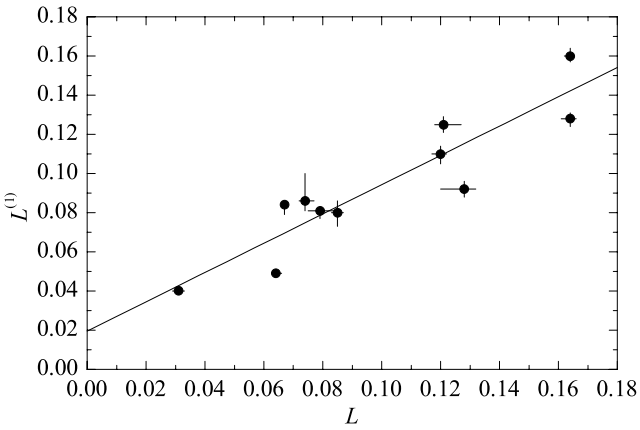

Fig. 7. The maximum LCEs computed by different methods; 11 satellites; the spatial case.

are taken from Table 2 and those of L from Table 1. The "whiskers" attached to the data points (in this and all the following graphs) reflect the maximum deviations of the current value of LCE from its mean value on the interval of averaging ($t \in [5 \times 10^4, 10^5]$ for the planar case, and $t \in [5 \times 10^5, 10^6]$ for the spatial case) on the LCE saturation plateau.

The straight line drawn in the graph is the linear fit $L^{(1)} = A \cdot L + B$). A good agreement of the results obtained by both methods is seen; the slope of the line (A) is 0.99 ± 0.07, the intercept (B) is 0.002 ± 0.004. The deviations given correspond to a confidence level of 95%.

In Fig. 7, the same graph is drawn for the case of spatial rotation. The values of $L^{(1)}$ are taken from Table 4, those of L from Table 3. The slope of the linear fit is 0.75 ± 0.11, the intercept is 0.02 ± 0.01. We see that the statistical agreement in the spatial case is worse than in the planar one. This is what one would expect, since the topology of the chaotic motion is much more complicated, and the simple shadow trajectory method is then apparently less suitable.

Compared to the planar case, significantly longer integration time is necessary to obtain correct estimates of the Lyapunov exponents. The trajectory in the spatial case is more complicated, it explores various regions of phase space with different local LCE values. In both methods, the total integration time is limited by the accumulation of errors. In the shadow trajectory method, the accumulation is caused by renormalizations, while in the HQR method it is conditioned by the difference between the exact tangent map matrix and its numerical approximation given by Eq. (15) or Eq. (17).

Let us now address the important question: can the theory for analytical estimation of maximum LCEs described above, apparently valid in the planar case, be used in the case of spatial rotation? A graph comparing maximum LCEs L_1 in the two cases is illuminating in this respect. It is presented in Fig. 8. One can see that there is no correlation.

It is interesting to note that in the cases of L_2 and L_3 global correlations between planar and spatial cases apparently exist (see Figs. 9, 10), though the dependences are not linear.

However, for the maximum LCE evidently the orbital eccentricity, and consequently the synchronous resonance, is of little importance in the spatial dynamics for a major fraction of our satellites; large-scale chaos is caused by the interaction of coupling resonances, which is already present in the circular problem. However, there is a range of values of the orbital and inertial parameters where our planar theory could still be valid. This range corresponds to a situation in which spin-orbit resonances are relatively important compared to internal coupling resonances. Intuitively, this situation could be achieved in two different ways. First, one can take a satellite almost dynamically-symmetric; then interaction of internal coupling resonances is suppressed. Second, one can take a satellite moving in a sufficiently eccentric orbit (note however that the eccentricity cannot be taken too great, say $e > 0.1$, since then our approximation of the Hamiltonian used to derive analytical LCE estimates is invalid); then the spin-orbit resonances are enhanced. Or, one can do both things at one and the same time.

Inspection of Tables 1–4 confirms our intuitive expectations. Let us take the two satellites with A/C maximum in our set. These are Proteus and Helene. Next let us take the two satellites with e maximum in our set. These are Hyperion and Phobos. We see that for these four satellites the agreement between maximum LCEs in the planar and spatial cases is indeed the best in the set. The other seven satellites behave much worse. The possible exception is the case of Epimetheus, where some agreement is observed; however, this may be accidental.

Comparing the values of the parameters of the satellites in our set, we infer that the validity limits of the theory are, very approximately, $e > 0.02$ and $A/C > 0.8$. If a satellite has parameter values outside this range, the external resonances involving explicit dependences on time play little role in the rotational dynamics; interaction of coupling resonances already prominent in the circular problem (since the satellite is significantly asymmetric) is of major importance. The corresponding Hamiltonian system is then close to autonomous. To proceed with analytical estimates of maximum LCEs in this case, one should deduce which of the internal coupling resonances is guiding (for the definition of a guiding resonance see Chirikov 1979). Another way to make progress in theoretical estimation here is to investigate the dependence of the maximum LCE on the energy of the system in the anti-integrable limit.

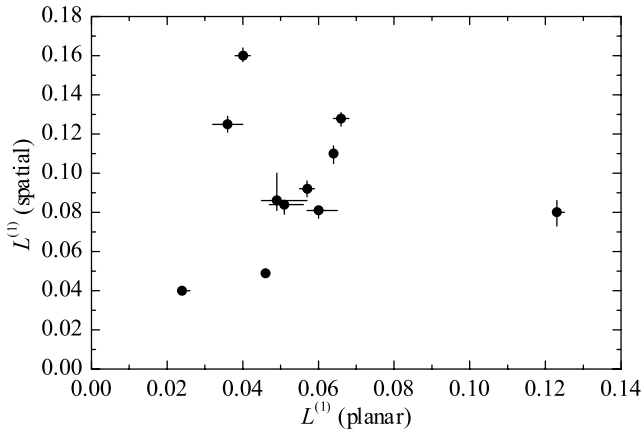

Fig. 8. L_1; planar and spatial.

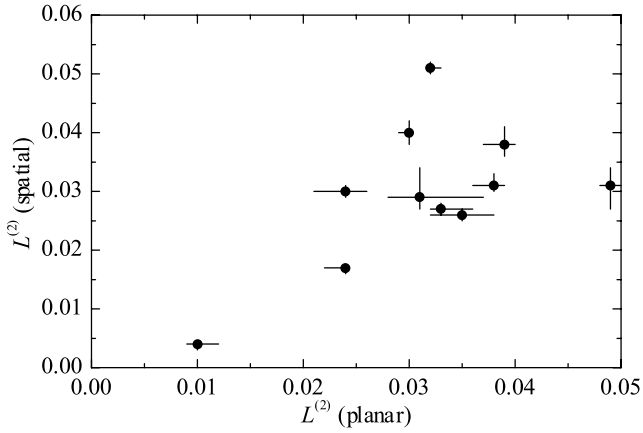

Fig. 9. L_2; planar and spatial.

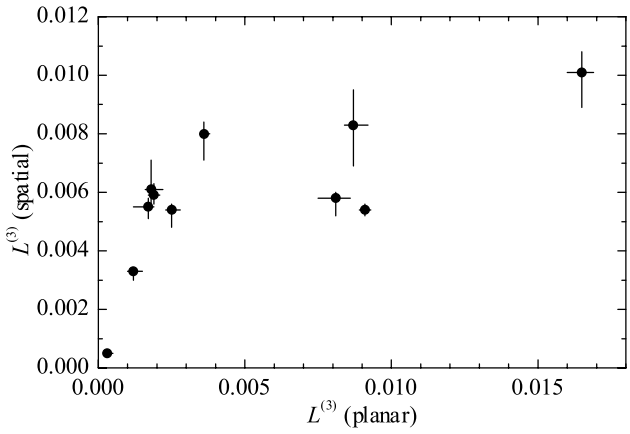

Fig. 10. L_3; planar and spatial.

Let us now consider the statistical relations between the components of the Lyapunov spectra, following from the data in Tables 2 and 4. The corresponding dependences are shown in Figs. 11 and 12. In these figures, the squares stand for the estimates of $L^{(2)}$ versus $L^{(1)}$, and the triangles for $L^{(3)}$ versus $L^{(1)}$. As one can see from Figs. 11 and 12, the values of the components are approximately proportional to each other.

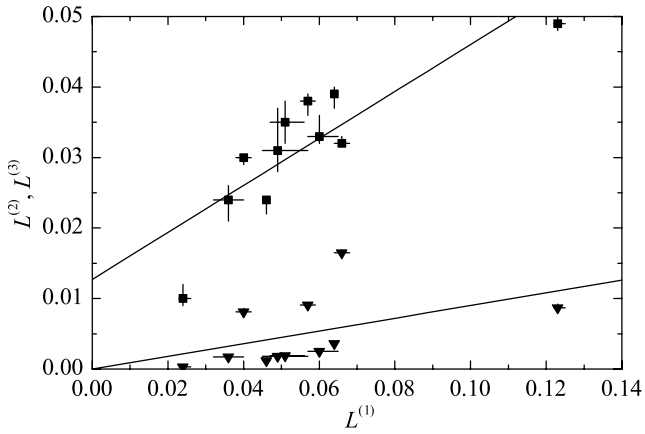

Fig. 11. Relations between the components of the Lyapunov spectra; the planar case.

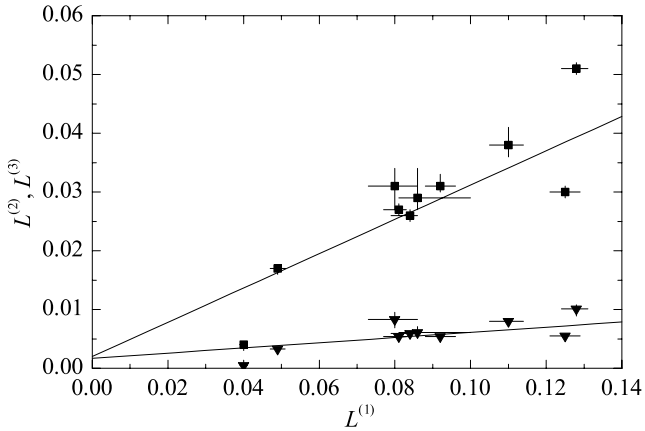

Fig. 12. Relations between the components of the Lyapunov spectra; the spatial case.

The proportionality is observed in both the planar and spatial cases. The average (over all satellites) ratios of the components of the Lyapunov spectra are $L^{(1)}/L^{(2)} \approx 1.8$, $L^{(1)}/L^{(3)} \approx 24$, and $L^{(2)}/L^{(3)} \approx 13$. The 95% confidence intervals are $[1.53, 2.06]$, $[9.68, 38.4]$, and $[6.74, 19.2]$, respectively. The average ratios of LCEs in the spatial case are $L^{(1)}/L^{(2)} \approx 3.7$, $L^{(1)}/L^{(3)} \approx 22$, and $L^{(2)}/L^{(3)} \approx 5.4$, the 95% confidence intervals being $[2.31, 5.18]$, $[8.61, 35.3]$, and $[4.56, 6.15]$, respectively.

In conclusion, we give results of the linear regression analysis for components L_1, L_2, L_3 of the Lyapunov spectra versus inertial parameters A/C, B/C and ω_0. These relations may be helpful while the theory for Lyapunov exponents in this problem is not yet completed. The linear fit coefficients are given with their 95% confidence range boundaries; R is the correlation coefficient.

$$L_1 = -(0.149 \pm 0.145)\frac{A}{C} + (0.194 \pm 0.100),\ R = -0.61,$$

$$L_2 = -(0.177 \pm 0.027)\frac{A}{C} + (0.081 \pm 0.018),\ R = -0.91,$$

$$L_3 = -(0.016 \pm 0.006)\frac{A}{C} + (0.017 \pm 0.004),\ R = -0.90,$$

$$L_1 = -(0.459 \pm 0.487)\frac{B}{C} + (0.503 \pm 0.434),\ R = -0.58,$$
$$L_2 = -(0.142 \pm 0.178)\frac{B}{C} + (0.156 \pm 0.159),\ R = -0.52,$$
$$L_3 = -(0.027 \pm 0.038)\frac{B}{C} + (0.030 \pm 0.034),\ R = -0.47,$$
$$L_1 = (0.065 \pm 0.091)\omega_0 + (0.044 \pm 0.073),\ R = 0.48,$$
$$L_2 = (0.039 \pm 0.021)\omega_0 + (0.000 \pm 0.017),\ R = 0.82,$$
$$L_3 = (0.008 \pm 0.004)\omega_0 + (0.000 \pm 0.004),\ R = 0.82.$$

The best correlations are observed in the case of A/C. This is understandable, since the moments of inertia are defined in such a way that $A < B < C$; so, A/C characterizes the maximum asymmetry. In the case of B/C the correlations are much worse. The case of ω_0 ought to be most relevant, generally speaking, to the planar case. Inasmuch as ω_0 depends on both A/C and B/C, the correlation has an intermediate character, averaging the cases of A/C and B/C. In the cases of A/C and ω_0, one should note that the correlations are better for the spectral components of higher order. This is again understandable, since for some satellites the role of the eccentricity is not negligible, and this affects mainly the maximum LCE.

7. Conclusions

In this paper, we considered the methods of numerical and analytical estimation of the maximum LCEs of the chaotic rotation of minor planetary satellites. The quantity reciprocal to the maximum LCE (the Lyapunov time) constitutes the characteristic time of predictable dynamics. In the application to studies of the rotational dynamics of planetary satellites, calculations of this quantity are helpful in planning observations of lightcurves of satellites whose rotational dynamics are chaotic or not yet known.

Our model comprises an asymmetric (tri-axial) rigid body rotating around its mass center and moving in a fixed elliptic orbit. We studied both planar and spatial rotation. In the planar case, the axis of rotation of a satellite coincides with the axis of its maximum moment of inertia and is orthogonal to the plane of the orbit. In the spatial case, the satellite may rotate in any direction.

The full Lyapunov spectra of the chaotic motion of 11 selected satellites, whose inertial and orbital parameters are known from observations, were computed in our model settings. The QR-based algorithm (von Bremen et al. 1997) was employed. We also used a more traditional "shadow trajectory" method which allows one to compute only the maximum LCE. For the maximum LCEs, the results obtained by the two methods are in good agreement.

Can the values of LCEs be predicted analytically in the problem considered? In order to investigate this problem, we considered applications of the analytical method based on the separatrix map theory (Shevchenko 2000a, 2002). We gave further evidence that this method provides a good description of the actual values of maximum LCEs in the planar problem (cf. Figs. 1 and 2).

Analytical estimation of the LCE spectrum in the spatial problem in the whole range of values of the inertial and orbital parameters remains a major challenge. At the present moment, only maximum LCEs in some intervals of these values can be analytically calculated; viz., in the case of minimum (in our set of satellites) dynamical asymmetries or/and maximum orbital eccentricities, the method by Shevchenko (2000a, 2002) seems to be applicable. In this case, synchronous resonance is guiding, and the separatrix map theory developed in application to the motion near separatrices of this resonance provides estimates of maximum LCEs which approximately agree with the numerical results.

The opposite situation requires a different approach. In the case of sufficiently large dynamical asymmetries and small orbital eccentricities, the role of external resonances involving explicit dependences on time is negligible in comparison with internal coupling resonances. In order to proceed with analytical estimates of maximum LCEs in this case, one should deduce which of the internal resonances is guiding.

We derived simple statistical dependences of the components of the LCE spectrum on the parameters of the problem. While a complete theory is lacking, these dependences may be helpful.

Acknowledgements. We thank Dr. A. V. Melnikov for valuable discussions. We are grateful to Dr. D. J. Scheeres for useful comments on the manuscript. This work was supported by the Russian Foundation for Basic Research (project number 01-02-17170).

References

Abdullaev, S. S., & Zaslavsky, G. M. 1995, Phys. Plasmas, 2, 4533
Abdullaev, S. S., & Zaslavsky, G. M. 1996, Phys. Plasmas, 3, 516
Ahn, T., Kim, G., & Kim, S. 1995, Physica D, 89, 315
Beletsky, V. V. 1965, The Motion of an Artificial Satellite about Its Mass Center (Nauka, Moscow) (in Russian)
Beletsky, V. V. 1981, Celest. Mech., 23, 371
Benettin, G., Galgani, L., & Strelcyn, J.-M. 1976, Phys. Rev. A, 14, 2338
Black, G. J., Nicholson, P. D., & Thomas, P. C. 1995, Icarus, 117, 149
von Bremen, H. F., Udwadia, F. E., & Proskurowski, W. 1997, Physica D, 101, 1
Burša, M. 1990, Bull. Astron. Inst. Czech., 41, 104
Celletti, A. 1990, Z. Angew. Math. Phys., 41, 174
Chirikov, B. V. 1977, Nonlinear Resonance (Izdatel'stvo NGU, Novosibirsk) (in Russian)
Chirikov, B. V. 1978, Interaction of Nonlinear Resonances (Izdatel'stvo NGU, Novosibirsk) (In Russian)
Chirikov, B. V. 1979, Phys. Rep., 52, 5, 263
Devyatkin, A. V., Gorshanov, D. L., Gritsuk, A. N., et al. 2002, Astronomiceskij Vestnik, 36, No. 3, in press (in Russian; English translation to appear in Solar System Research)
Éphémérides Astronomiques 1995 (Annuaire du Bureau des Longitudes) (Masson, Paris)
Goździewski, K., & Maciejewski, A. J. 1995, Earth, Moon and Planets, 69, 25
Hairer, E., Nørsett, S. P., & Wanner, G. 1987, Solving Ordinary Differential Equations I. Nonstiff Problems (Springer-Verlag, Berlin)
Holman, M. J., & Murray, N. W. 1996, AJ, 112, 1278
Klavetter, J. J. 1989, AJ, 98, 1855
Lichtenberg, A. J., & Lieberman, M. A. 1992, Regular and Chaotic Dynamics (Springer-Verlag, New York)

Meiss, J. D. 1992, Phys. Rep., 64, 795
Melnikov, A. V., & Shevchenko, I. I. 1998, Solar System Res., 32, 480
Melnikov, A. V., & Shevchenko, I. I. 2000, Solar System Res., 34, 434
Murray, N. W., & Holman, M. J. 1997, AJ, 114, 1246
Peale, S. J. 1977, in Planetary Satellites, ed. J. A. Burns (Univ. of Arizona Press, Tucson), 87
Pesin, Ya. B. 1976, Doklady Akademii Nauk SSSR, 226, 774 (in Russian)
Shevchenko, I. I. 1998, Phys. Scr., 57, 185
Shevchenko, I. I. 1999, Celest. Mech. Dyn. Astron., 73, 259
Shevchenko, I. I. 2000a, Izvestia GAO, 214, 153 (in Russian)
Shevchenko, I. I. 2000b, J. Exp. Theor. Phys., 91, 615 (English translation)
Shevchenko, I. I. 2000c, in The Chaotic Universe, ed. V. G. Gurzadyan, & R. Ruffini (World Scientific, London), 599
Shevchenko, I. I. 2002, Cosmic Research, 40, 296 (English translation)
Simonelli, S. P., Thomas, P. C., Carcich, B. T., et al. 1993, Icarus, 103, 49
Smith, B. A., Soderblom, L., Batson, R., et al. 1982, Science, 215, 504
Tancredi, G., Sánchez, A., & Roig, F. 2001, AJ, 121, 1171
Thomas, P. C., Black, G. J., & Nicholson, P. D. 1995, Icarus, 117, 128
Treschev, D. V. 1998, Introduction to the Theory of Perturbations of Hamiltonian Systems (Fazis, Moscow) (In Russian)
Vecheslavov, V. V. 1996, J. Exp. Theor. Phys., 109, 2208 (in Russian)
Vecheslavov, V. V. 1999, Physica D, 131, 55
Wisdom, J. 1983, Icarus, 56, 51
Wisdom, J. 1987, AJ, 94, 1350
Wisdom, J., Peale, S. J., & Mignard, F. 1984, Icarus, 58, 137